ACS OMEGA

Open Access

http://pubs.acs.org/journal/acsodf

Article

Enhanced Polyacrylamide Degradation via OH Radical-Initiated Single-Electron Transfer

Jun Zhang,[♦] Ming Hao,[♦] Depeng Zhang,[♦] Xuesong Zhang, Shijun Guo, Bo Wang, Junping Xiao,* Yang Gao,* and Xiaoan Li*

Cite This: *ACS Omega* 2023, 8, 46589−46597

Read Online

ACCESS | Metrics & More | Article Recommendations | Supporting Information

ABSTRACT: Hydroxyl (OH) radicals, as common radicals in aqueous environments, play an important role in inducing the degradation reactions of polymers. However, understanding the fundamental mechanisms of radical-induced degradation of polymers at the atomic level remains a formidable challenge. In this study, we employ density functional theory to investigate the geometric and electronic structural properties of polyacrylamide (PAM) in $(-CH_2CHCONH_2-)_n$ (n = 2−6) complexes. Additionally, we explore the degradation mechanism of the n = 4 complex induced by the OH radical. The results indicate that there are three sites for the initial reaction (R1 and R2 are at the ends and R3 is in the middle). The OH radical removes a H atom from the PAM main chain and simultaneously triggers a single-electron-transfer process on the same chain. This process significantly reduces the dissociation energy barrier of the C−C bond in the PAM chain, from ∼90 to ∼20 kcal/mol. Specifically, when the induced reaction occurs at the end of the chain, a series of broken bonds will appear only along the main chain. While it happens in the middle, the broken bonds will exist simultaneously along both the main and side chains. Our results reveal the importance of OH radicals in polymer dissociation, particularly in PAM, and emphasize the degradation mechanism of SET.

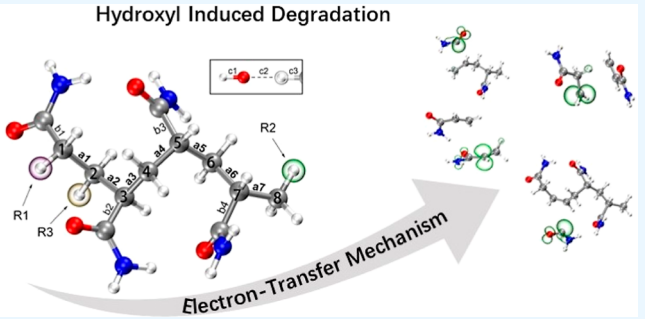

INTRODUCTION

Radicals play an important role in many chemical reactions because of their unpaired single electron, which makes them highly reactive, thus easily attacking the substrate, destroying their stable electronic structure of the substrate by snatching electrons, and making them easily reaction activated.[1−4] The interaction of radicals with polymers is considered to be one way of polymer degradation, which will induce the production of unpaired single electrons in the polymer, and then the electron transfer causes the polymer degradation.[5,6] Therefore, the role of radicals in the polymer reaction cannot be ignored, especially in a solution environment. For highly polymerized organic molecules such as polyethylene (PE),[7] polyvinyl chloride (PVC),[8] polyacrylamide (PAM),[9] poly-a-methylstyrene (PAMS), etc., radicals may be even more important because their chain structure provides the possibility of continuous electron transfer for the reaction in thermodynamics and chemistry. In addition, specific polymers will exhibit their own degradation properties. It has been reported that in some polymers, the unsaturated end of the chain will significantly reduce the degradation energy barrier of the polymer, and the way that the monomer unit is connected can also influence the difficulty of degradation.[10] This reflects the complexity of the polymer degradation mechanism.

PAM is widely used in petroleum exploitation,[11] water treatment,[12] mineral processing,[13] paper making,[14] and so on.[15] Its application value determines the importance of clarifying and grasping its nature. Up to now, although a lot of experiments have recognized its degradation properties and put forward many hypotheses on its mechanism, there are relatively few theoretical studies on radical-induced degradation, hence the theoretical explanation of its reaction mechanism on radical-induced electron-transfer degradation is still unclear. For example, the process of degradation of PAM occurs in two steps and finally releases ammonia.[16] It has also been found that light is a factor that causes the PAM degradation to break the C−C bond,[17,18] and the photocatalytic degradation of hydrolyzed PAM can be achieved by aligned zinc oxide nanorods (ZnO NRs).[19] In addition, the maximum chemical oxygen demand and the removal rate of PAM wastewater by Fenton oxidation and anaerobic organisms approach can reach 94.61 and 91.06%, respectively.[20]

Received: July 29, 2023
Revised: November 2, 2023
Accepted: November 10, 2023
Published: November 29, 2023

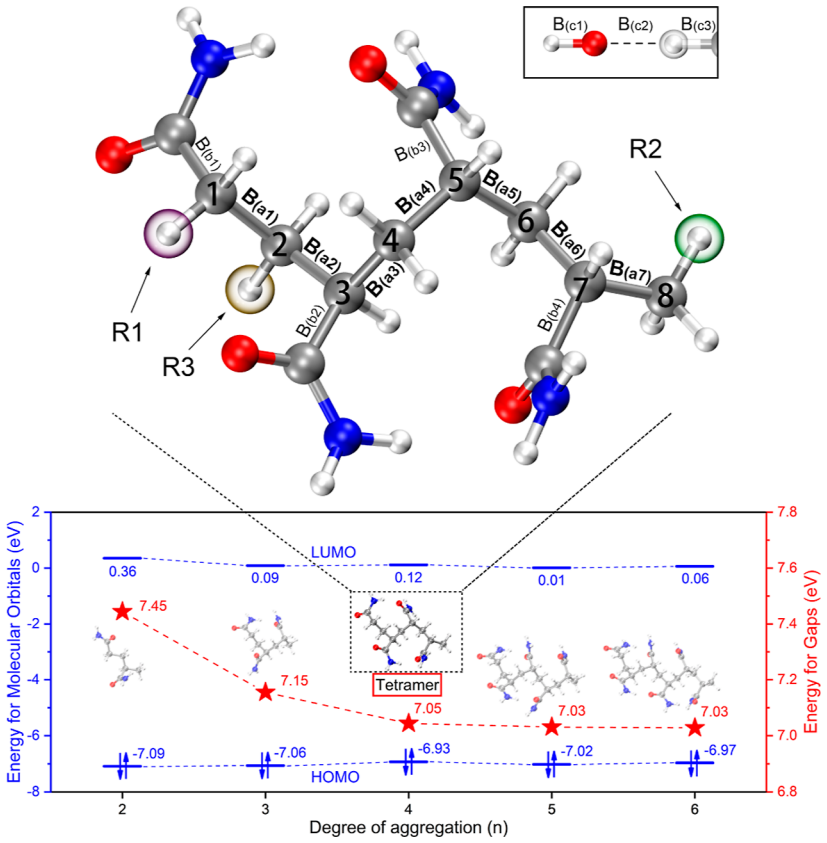

Figure 1. Optimal geometries and the electronic structure of the PAM degrees of aggregation (n = 2−6). The top half shows the structure and three potential reactive sites (purple: R1, green: R2, yellow bubbles: R3) of the tetramer saturated by H atoms. The C−C bonds in the main chain are marked by a1−a7 and those on the side chain as b1−b4. The upper right schematic diagram shows the orientation when the OH radical attacks the H atom at the corresponding reactive sites on the PAM. The related interatomic distances are marked by c1−c3. The lower part indicates the energy states of the polymers with the degrees of aggregation (n = 2−6). The blue stubs are the energy for HOMO and LUMO and the red ones are the energy gap.

However, how the radicals induce the electron transfer along the PAM chain and lead to degradation and to what extent they affect the difficulty of degradation in terms of energy and electronic structure are not yet clear. PAM is a linear polymerization structure, has a similar degradation mechanism as that of general hydrocarbon polymers,[21−23] but with different side-chain groups, which makes the reaction of PAM also specific.[24−26] Therefore, it is necessary to carry out research to reveal the theoretical reaction mechanism on the radical-induced electron-transfer degradation of PAM.

Based on the above existing problems, we systematically studied the interaction between the common OH radical and different reactive sites of PAM by using first-principles density functional theory (DFT) with empirical dispersion correction. In order to test the relationship between the length of the chain and the property, we considered the polymers composed of 2−6 monomer units $(-CH_2CHCONH_2-)_{n=2-6}$, and a typical tetramer (n = 4) was selected as the typical polymer because its electronic structural properties (HOMO−LUMO gap) (HOMO = highest occupied molecular orbital; LUMO = lowest unoccupied molecular orbital) is very similar to those of longer polymers (n = 5,6). In this paper, the degradation reaction was explored from the aspects of potential energy surface (PES), interaction energy, spin polarization, charge transfer, and chemical bond breaking. It is found that the single-electron transfer (SET) process is the key point of degradation mechanism induced by attacking of radicals on PAM. We hope to understand the internal mechanism of the degradation of PAM under the action of radicals and provide help for the purification of oily sewage, preparation/preservation of coagulants, etc.

COMPUTATIONAL METHODS

The exploration of the degradation mechanism of PAM was done by first-principles DFT. PAMs with degrees of polymerization ranging from 2 to 6 were modeled with both ends of initial PAMs saturated with hydrogen atoms, so that all electrons were paired. To choose an appropriate method, five commonly used methods (PBE,[27] B3LYP,[28] M06-2X,[29] TPSSh,[30] and LC-wPBE[31]) were used to optimize the geometrical structures. In different levels of DFT methods, hybrid functionals such as B3LYP can provide the result of relatively accurate geometric and electronic structures, which can be compared to ab initio second-order perturbation methods at the computational level.[32−34] Particularly, with the gradual development of dispersion correction methods, it compensates for the possible shortcomings of different DFT methods in handling intermolecular interactions. Currently, dispersion-corrected DFT has been proven to have sufficient reliability in degradation or many chemical reactions and can even achieve high-precision agreement with experiments.[35−37]

In this work, the hybrid generalized gradient approximation functional with empirical dispersion correction B3LYP-D3[38,39] was used, which makes it widely accepted as the proper

https://doi.org/10.1021/acsomega.3c05548
ACS Omega 2023, 8, 46589−46597

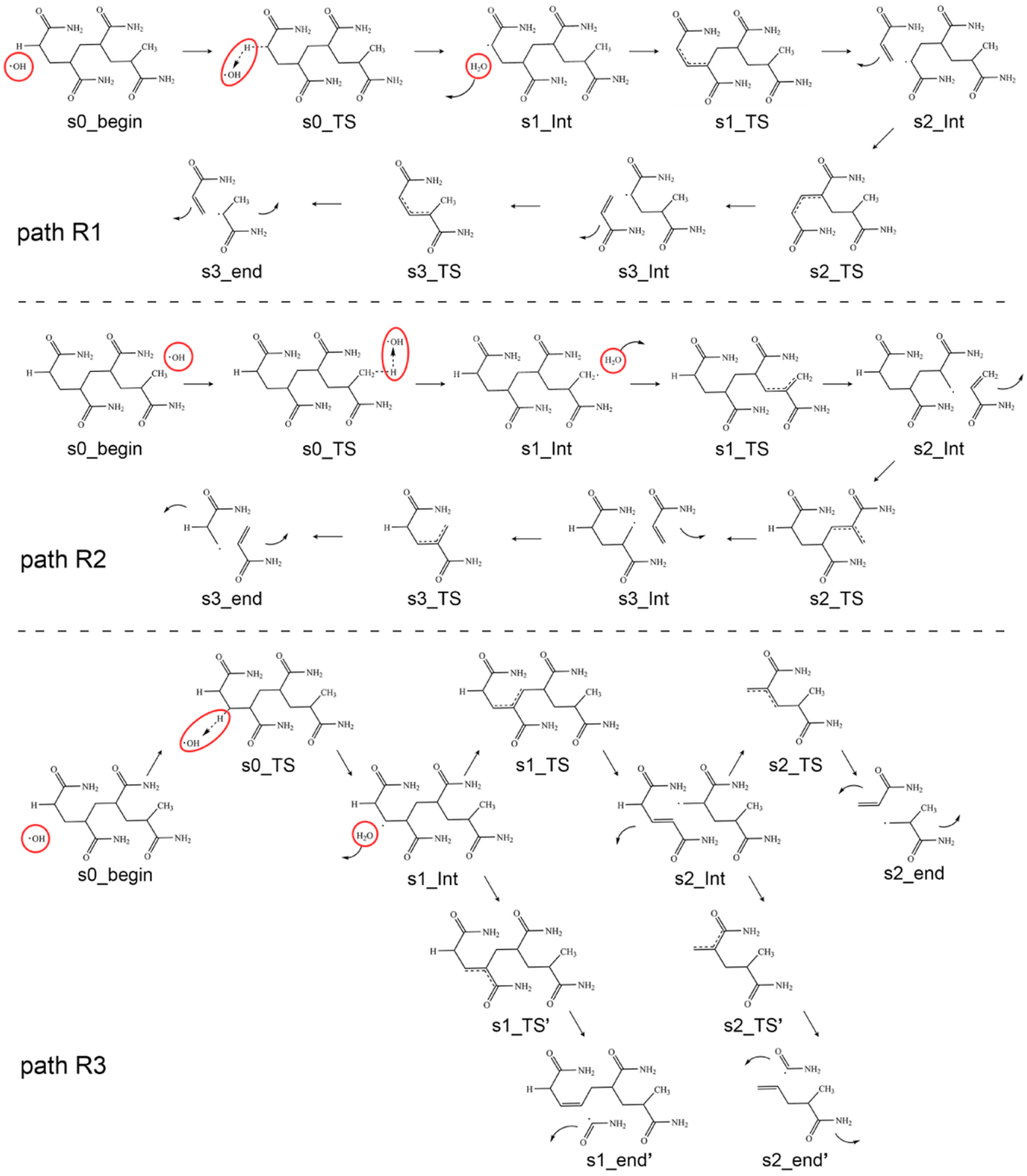

Figure 2. Schematic diagrams of the R1, R2, and R3 reactions. The reactive sites are circled in red. The first letter of the name stands for the step, and its apostrophe mark in the upper right corner represents the reaction of side-chain breaking to distinguish it from the reaction of main chain breaking. TS and Int represent transition and intermediate states, respectively.

functional to study the interaction between polymer molecules.[40] A triple-ζ 6-311G(d,p) basis set[41,42] was employed to describe the system wave function. For all of the calculations, solvation model based on density (SMD) methods were used with water as the solvent.[43] The vibration frequency of the optimized stable structure was calculated at the same level to obtain thermochemical corrections as well as to ensure that all structures correspond to local minima. The transition state (TS) theory method can search the local transition state according to the structure initially guessed by experience in the Berny algorithm, and the TS can be determined by the vibrational frequency, and only one virtual frequency exists. Then, the calculation of intrinsic reaction coordinates (IRCs)[44,45] was employed to trace the reaction path on the PES. All the calculations were performed in the Gaussian09 revision D.01 package.[46]

RESULTS AND DISCUSSION

The size effect of the PAM polymer decreases with the increase of polymerization degree, which can be reflected in its electronic structure properties. By comparing the energy-level positions of HOMO and LUMO (i.e., the HOMO−LUMO

https://doi.org/10.1021/acsomega.3c05548
ACS Omega 2023, 8, 46589−46597

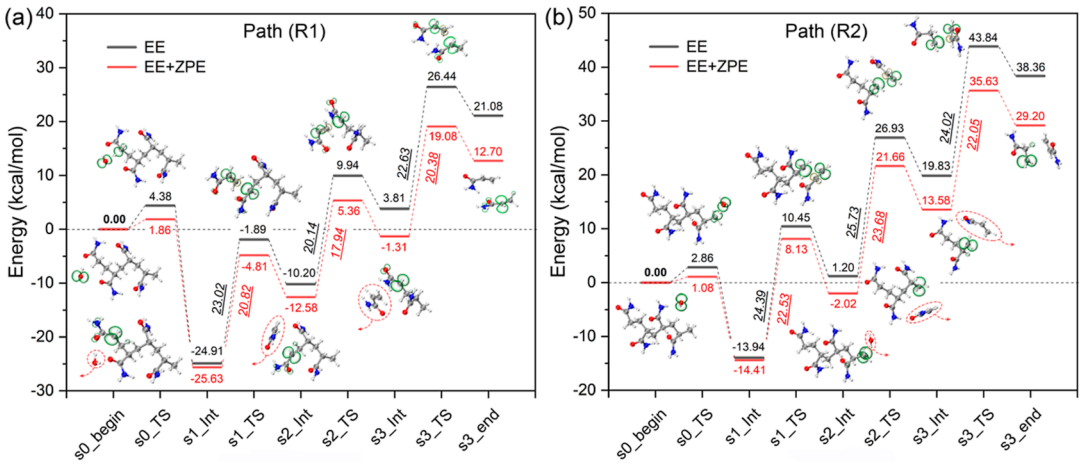

Figure 3. Optimized geometries and transfer processes of spin polarization density in the R1 (a) and R2 (b) reaction paths along the PES. The energies of the corresponding structures without and with zero-point energy (ZPE) are shown by black and red lines, respectively. The green and yellow bubbles represent upward and downward spins, respectively (isovalue = 0.01). The analysis results and conclusions will not be affected with or without ZPE correction which has been discussed below, so the results without ZPE correction are mainly discussed in this paper.

gap), we determined that the tetramer (n = 4) with four acrylamide monomer structural units ($-CH_2CHCONH_2-$) can simulate the electronic structural properties of the PAM polymer. Figure 1 shows the optimal geometries and electronic structure results of PAMs with degrees of polymerization ranging from 2 to 6. Although LUMO and HOMO energies vary irregularly with increasing degree of polymerization, the HOMO−LUMO gap decreases along with increasing degree of polymerization. When the degree exceeds n = 4, the HOMO−LUMO gap tends to be flat, and the gap value stabilizes around 7.05 eV. This indicates that the PAM with the degree of polymerization (n = 4) can be adopted to represent the properties of PAMs with a higher degree of polymerization. Therefore, we will focus on the study of the tetramer (n = 4) structures.

In addition, different DFT methods such as PBE, M06-2X, TPSSh, and LC-wPBE were also used to repeat the above calculations, obtaining the same optimal structures and the similar variation of the gap value along with the degree of polymerization, which verified the reliability of the method we used above (see Part 1 of the Supporting Information). To assist in experiments, providing specific vibrational information resulting from size effects, we calculated the infrared spectra for n = 2 to 6. The results indicate that the infrared spectra of PAMs with varying values of n exhibit a high degree of similarity. The distribution patterns of characteristic peaks remain largely consistent across the entire range of n (see Part 2 of the Supporting Information). This observation suggests that the impact of the PAM size on the distribution of characteristic peaks within the IR spectrum is negligible and not discernible. However, based on further calculations and the obtained dipole moment data for PAMs (n = 2 to 6), we observed that when n = 4 (μ = 16.20 D), the dipole moment suddenly increases significantly compared to n = 2 (μ = 2.47 D) and n = 3 (μ = 7.62 D), even surpassing n = 5 (μ = 15.49 D). This finding strongly implies that PAM (n = 4) may be the most stable among these polymer segments, potentially playing a crucial role as a monomer in the polymer precipitation process (see Part 3 of the Supporting Information). This result provides us with deeper insights, suggesting that PAM (n = 4) might be a promising choice for selectively precipitating polymers of specific sizes.

Based on the structural features of PAM and the calculation results of transition states and reaction paths, we found that the OH radical readily attacks the H atoms in the end of the PAM chain or in the methylene groups, which can generate water molecules and make the unpaired single-electron appear at the C atoms in the end or middle of the PAM chain. In fact, we also considered the direct attack of OH radicals on the C−C main chain and the H atoms in $-NH_2$ and found that the probabilities of these events are both very low. For details, please refer to the Supporting InformationParts 4 and 5.

From the perspective of the reactive sites of the hydroxyl attacking PAM (Figure 1), it can be summarized as three different reactions, namely, R1, R2, and R3. A schematic diagram of the reactions (R1, R2, and R3) is shown in Figure 2. R1 and R2 represent the OH radical attack at the methylene and methyl groups in the PAM chain, respectively. R3 represents the hydroxyl group attack at the methylene groups in the middle C atom of the PAM chain. After the H atom of PAM is robbed by an OH radical in any of these three reactions, the unpaired single electron is thus localized in a C atom of the PAM chain, which appears as an increase in the electron spin density at this atom. In this case, the single bond between a single-electron C atom and its adjacent C atom tends to form a double bond through the rearrangement of electrons, accompanied by a bond breaking, occurring on the single bond between the adjacent C atom and the subsequent C atom. Thus, the single electron is transferred along the chain, accompanied by continuous bond breaking along the PAM chain. The specific mechanism of the SET can also be manifested as a spin-transfer reaction. The depolymerization mechanisms of the three reactions are discussed in detail below.

R1 represents a series of degradation reactions caused by dehydrogenation of the left-end methylene $-CH_2-$ group by OH radicals, as shown in Figures 2 and 3. The first step is to induce a reaction where the OH radical is attached to the H atom of the $-CH_2-$ group. The electronegative O atom in the OH radical can easily drag the H atom from PAM and combine with it to generate a water molecule. Therefore, the spin density of the unpaired single electron in the OH radical is transferred to the $C_{(1)}$ atom (number 1 carbon atom in Figure 1) that has lost an H atom (see Figure 3a, s1_Int). In the

https://doi.org/10.1021/acsomega.3c05548
ACS Omega 2023, 8, 46589−46597

Table 1. Summary of the Wiberg Bond Orders of Chemical Bonds Involved in the R1 Reaction Pathway

	s0_begin	s0_TS	s1_Int	s1_TS	s2_Int	s2_TS	s3_Int	s3_TS	s3_end
$B_{(c1)}$	0.73	0.76	0.72						
$B_{(c2)}$	0.00	0.24	0.75						
$B_{(c3)}$	0.91	0.64	0.00						
$B_{(a1)}$	1.00	1.01	1.07	1.61	1.92				
$B_{(a2)}$	0.99	0.99	0.98	0.30	0.00				
$B_{(a3)}$	0.98	0.99	0.99	1.05	1.07	1.58	1.91		
$B_{(a4)}$	0.99	0.99	0.99	0.99	0.99	0.32	0.00		
$B_{(a5)}$	1.00	1.00	1.00	1.00	1.00	1.05	1.07	1.62	1.93
$B_{(a6)}$	0.99	0.99	0.99	0.99	0.99	0.99	0.99	0.29	0.00
$B_{(a7)}$	1.00	1.00	1.00	1.00	1.00	1.01	1.01	1.08	1.10

Table 2. Summary of the Wiberg Bond Orders of Chemical Bonds in the R1 Reaction Pathway

	s0_begin	s0_TS	s1_Int	s1_TS	s2_Int	s2_TS	s3_Int	s3_TS	s3_end
$B_{(c1)}$	0.80	0.79	0.77						
$B_{(c2)}$	0.00	0.19	0.75						
$B_{(c3)}$	0.94	0.71	0.02						
$B_{(a1)}$	1.00	1.00	1.00	1.00	1.00	1.00	1.00	1.06	1.08
$B_{(a2)}$	0.99	0.99	0.99	1.00	0.99	0.98	0.98	0.28	0.00
$B_{(a3)}$	0.98	0.98	0.99	0.99	0.99	1.04	1.05	1.63	1.93
$B_{(a4)}$	0.99	0.99	0.99	0.99	0.97	0.30	0.00		
$B_{(a5)}$	1.00	1.00	1.00	1.05	1.05	1.62	1.94		
$B_{(a6)}$	0.99	0.99	0.99	0.33	0.01				
$B_{(a7)}$	1.00	1.00	1.04	1.59	1.92				

meantime, because of the SET processes, the hybridization and bonding types of the $C_{(1)}$ atom will also change accordingly.

Specifically, the chemical bond $B_{(a1)}$ between $C_{(1)}$ and $C_{(2)}$ changes from a single bond to a double bond (1.07 → 1.92, Table 1), and the chemical bond $B_{(a2)}$ between $C_{(2)}$ and $C_{(3)}$ breaks (0.98 → 0.00, Table 1), accompanied by the dropping of an acrylamide monomer (see Figure 3a, s1_Int−s2_Int). After this step, the single electron on the $C_{(1)}$ atom will be transferred to the $C_{(3)}$ atom, which continues to reproduce the previous SET processes. This allows the single electron to be transferred along the main chain and the monomers to drop off one by one. The whole degradation process can be divided into four steps (since the computational model we choose is a tetramer). After being attacked by the hydroxyl group, the PAM degraded the monomers in sequence through a three-step bond-breaking reaction and finally generated four monomer molecules.

In the analysis of PES, the energy barriers are calculated, and the electronic energy of the system is corrected with a zero-point energy (ZPE) by calculating the vibration frequency. Whether ZPE correction is considered has no effect on the conclusion. Therefore, we will focus on the discussion based on the energy without ZPE correction. Among the four steps of the degradation reaction (Figure 3a), the first step has the lowest energy barrier (4.38 kcal/mol) to overcome compared with the other three-step reaction (∼20 kcal/mol). Although the first step is relatively easy to induce, it plays a key role in the initiation of the degradation reaction of PAM. To give a clear comparison, we also forcibly break the chemical bond $B_{(a2)}$ between $C_{(2)}$ and $C_{(3)}$ on the PAM tetramer without single-electron transfer, and an energy barrier of about 90 kcal/mol is found to be overcome. (It requires 93.55 kcal/mol to stretch the $B_{(a2)}$ from 1.54 Å in the equilibrium state to 3.54 Å.) Induced by the SET processes, this reaction only needs to overcome the energy barrier of about 20 kcal/mol (reducing to around 25% of the original level). The remaining three steps have the same bond degradation mechanism and so have the almost same energy barriers to be overcome (about 20 kcal/mol). Considering the correction by zero-point vibration energy, the energy barrier of each step is decreased by 1 ∼ −2 kcal/mol, which does not affect the overall energy change law qualitatively. Therefore, it can be concluded that radical attack can serve as a catalytic means of PAM degradation.

The SET processes at the end of the chain can also proceed via the R2 reaction path, as shown in Figures 2 and 3b. The calculation results indicate that the H atom of the methyl group can be taken away by the OH radical. Therefore, the methyl carbon loses an H atom and becomes an unsaturated carbon, forming a single-electron-suspended bond on the methyl carbon. The energy barrier of the first step is 2.86 kcal/mol, which is lower than that in the R1 reaction path (4.38 kcal/mol). Despite the ZPE corrections having been done, there is no qualitative change between them (1.08 kcal/mol in R2 vs 1.86 kcal/mol in R1). This result reflects that the hydroxyl group is more likely to attack the right-end methyl group than the left methylene group during the degradation initiation process. In contrast to the direction of R1 degradation, R2's degradation comes from the other side of the chain. The C−C bonds $B_{(a7)}$, $B_{(a5)}$, and $B_{(a3)}$ changed from a single bond to a double bond, while the C−C bonds $B_{(a6)}$,

https://doi.org/10.1021/acsomega.3c05548
ACS Omega 2023, 8, 46589−46597

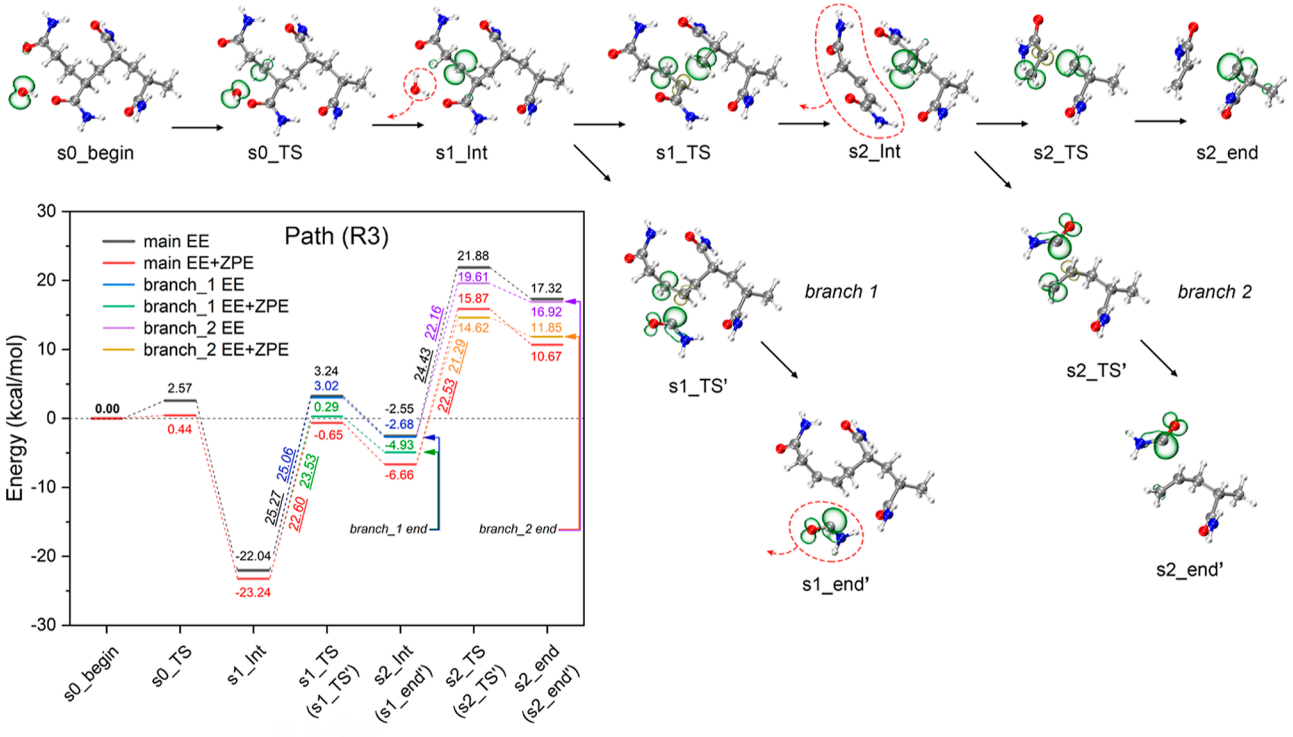

Figure 4. Optimized geometries and transfer processes of spin polarization density along the PES in the R3 reaction paths. The green and yellow bubbles represent different spin orientations (isovalue = 0.01).

Table 3. Summary of the Wiberg Bond Orders of Chemical Bonds in the R3 Reaction Pathway[a]

	s0_begin	s0_TS	s1_Int	s1_TS	s2_Int	s2_TS	s2_end	s1_TS'	s1_end'	s2_TS'	s2_end'
$B_{(c1)}$	0.75	0.77	0.74								
$B_{(c2)}$	0.01	0.15	0.73								
$B_{(c3)}$	0.92	0.74	0.00								
$B_{(a1)}$	1.00	1.00	1.05	1.03	1.03			1.03	1.02		
$B_{(a2)}$	1.00	1.00	1.04	1.58	1.85			1.63	1.91		
$B_{(a3)}$	0.99	0.98	0.97	0.28	0.00			1.02	1.03		
$B_{(a4)}$	0.99	0.99	0.99	1.04	1.05	1.64	1.93	0.97	0.97	1.68	1.93
$B_{(a5)}$	1.00	1.00	1.00	1.00	0.98	0.28	0.00	1.00	1.00	1.03	1.03
$B_{(a6)}$	0.99	0.99	0.99	0.99	1.00	1.04	1.05	0.99	0.99	0.98	0.97
$B_{(a7)}$	1.00	1.00	1.00	1.00	1.00	0.97	0.97	1.00	1.00	1.00	1.00
$B_{(b1)}$	0.99	0.98	0.97	0.98	0.98			0.97	0.97		
$B_{(b2)}$	0.97	0.96	0.93	1.02	1.04			0.26	0.01		
$B_{(b3)}$	0.97	0.97	0.97	0.96	0.97	1.02	1.03	0.97	0.97	0.25	0.00
$B_{(b4)}$	0.97	0.97	0.97	0.97	0.96	0.96	0.95	0.97	0.97	0.96	0.96

[a]The left part of the table lists the bond orders of PAM degradation alone the main chain, and the right parts are the first (s1′) and second (s2′) branching reactions parallel to the s1 and s2 reactions.

$B_{(a4)}$, and $B_{(a2)}$ are successively broken, as shown in Table 2. The sequential C−C bond cleavage in the R2 reaction path is also accompanied by a single-electron transfer, which can be seen from the spin-density transfer in Figure 3b. Finally, the entire PAM chain is degraded into monomers in a four-step process.

In addition to the two degradation reaction paths mentioned above (R1 and R2) that start from the ends of the PAM chain, the degradation can also begin in the middle of the chain to both sides (R3). In this case, the $-CH_2-$ (located in carbon atoms with numbers 2, 4, and 6 shown in Figure 1) can be attacked by the OH radical, and the related carbon atom loses an H atom and produces a single electron on itself. Taking the $C_{(2)}$ atom as a starting point, a single electron appears on $C_{(2)}$ after attacked by the OH radical (s1_Int in Figure 4). The chemical bond $B_{(a2)}$ between $C_{(2)}$ and $C_{(3)}$ on the main chain is easily activated by a single electron, which is directly related to the stability of the side chain and the main chain around the $C_{(3)}$ atom. Once the bond breaking occurs on the side chain, the exfoliated amide group will take away the single electron, and the remaining fragment will return to a saturated state where the spin density is transferred on the side chain in the

https://doi.org/10.1021/acsomega.3c05548
ACS Omega 2023, 8, 46589−46597

branch reaction paths (s1_end′, Figure 4). In this case, all electrons on the main chain are paired without a single electron, and the PAM changes into the inactive state. However, when the C−C bond breakage occurs on the main chain, the single electron is transferred to the remaining fragment of the PAM chain, which facilitates the next degradation. Consequently, cracking of PAM can be achieved (Table 3).

In reaction R3, the H atom is more easily taken away by the OH radical in the first step (energy barrier is 2.57 kcal/mol) than those in R1 (4.38 kcal/mol) and R2 (2.86 kcal/mol) reactions. Since the R3 reaction starts from the middle point of the PAM chain, the degradation process proceeds in two directions. Because the reactions from the middle point to the left end and to the right end are equivalent, it can be inferred that the degradation process can also be carried out from the middle point along the chain toward the left end of the chain. The SET processes along the main chain in reaction R3 are similar to those of reactions R1 and R2, so it also needs to overcome the energy barrier of around 20 kcal/mol for bond breaking. According to the statistics of energy barrier heights, the energy required for side-chain detachment is the same as that for the main chain, which means that both the monomer and side-chain detachment from the PAM chain are both major degradation steps.

In terms of the number of reactive sites to start the reaction, although the number of reactive sites in R3 is more than those of R1 and R2, the R1 and R2 reactions have their own advantages in their electron transport. In other words, neither reaction is affected by the breaking of the side chain and taken away by the single electron, avoiding inactivation of the chain and the suspension of the degradation reaction, which means that only one hydroxyl group is needed to initiate the whole degradation process. Although there are many initial reactive sites for reaction R3, the subsequent degradation of the remaining PAM chain stops once the side chains are detached. Therefore, reaction R3 requires many hydroxyl groups to restart the paused degradation reaction at any time.

CONCLUSIONS

In summary, the first-principles density functional theory is used to reveal a series of hydroxyl-radical-induced degradations of PAM caused by single electron-transfer. We found that the H atom of the PAM chain is easily (less than 5 kcal/mol) taken away by the hydroxyl radical via SET processes. The existence of the single electron activates the C−C bond, thus catalyzing C−C bond breaking and PAM degradation. Specifically, the appearance of a single electron lowers the dissociation energy barrier of the C−C bond to about 25% of its original value (from ∼90 to ∼20 kcal/mol). Moreover, the degradation of PAM begins at different reactive sites of PAM and proceeds along three degradation paths under the action of the hydroxyl radical. These paths will degrade the PAM into acrylamide monomers through the main chain breakage, and one of them can also degrade amide group fragments through progressive breakage of the PAM side chain during the SET processes. The above degradation paths can occur simultaneously in PAM aqueous solution, thus resulting in the acceleration of degradation of PAM. It is worth noting that while the single electron transfers along the chain induced by hydroxyl radicals are key to catalyzing the degradation of PAM, other potential external factors, such as variations in solvent, mixtures, pH levels, etc., concurrently influence the intricate degradation process of PAM. It is hoped that these findings will be helpful to further understand the nature of PAM and promote the realization of higher application value of PAM.

ASSOCIATED CONTENT

Supporting Information

The Supporting Information is available free of charge at https://pubs.acs.org/doi/10.1021/acsomega.3c05548.

Calculations of structures and gaps in different DFT methods; infrared spectra for n = 2 to 6; dipole moment data for PAMs (n = 2 to 6); direct attack of OH radicals on the C−C main chain; direct attack of OH radicals on the H atoms in $-NH_2$; coordinates of the optimized PAM (n = 2−6) structures; and coordinates of the PAM structures for Reaction 1, Reaction 2, and Reaction 3 (PDF)

AUTHOR INFORMATION

Corresponding Authors

Junping Xiao − *College of Physics and Electronic Information, Baicheng Normal University, Baicheng, Jilin 137000, China*; Email: djtc999@163.com

Yang Gao − *NHC Key Laboratory of Nuclear Technology Medical Transformation, Mianyang Central Hospital, School of Medicine, University of Electronic Science and Technology of China, Mianyang, Sichuan 621099, China; Institute of Fundamental and Frontier Sciences, University of Electronic Science and Technology of China, Chengdu, Sichuan 610054, China*; orcid.org/0000-0001-9148-8635; Email: ygaoxs@gmail.com, ygaoxs@uestc.edu.cn

Xiaoan Li − *NHC Key Laboratory of Nuclear Technology Medical Transformation, Mianyang Central Hospital, School of Medicine, University of Electronic Science and Technology of China, Mianyang, Sichuan 621099, China*; orcid.org/0009-0006-8293-8845; Email: lixiaoan@sc-mch.cn

Authors

Jun Zhang − *The Key Laboratory of Enhanced Oil and Gas Recovery of Educational Ministry, Northeast Petroleum University, Daqing 163318 Heilongjiang, China; Liaohe Operation Service Company of Liaohe Oilfield Company, Panjin, Liaoning 124100, China*

Ming Hao − *The Key Laboratory of Enhanced Oil and Gas Recovery of Educational Ministry, Northeast Petroleum University, Daqing 163318 Heilongjiang, China; Post-doctoral Working Station of Liaohe Oil Field, Panjin 124010 Liaoning, China*

Depeng Zhang − *Normal School, Shenyang University, Shenyang 110044, China*

Xuesong Zhang − *The Key Laboratory of Enhanced Oil and Gas Recovery of Educational Ministry, Northeast Petroleum University, Daqing 163318 Heilongjiang, China*

Shijun Guo − *College of Chemical Engineering, Daqing Normal University, Daqing 163712 Heilongjiang, China*

Bo Wang − *College of Science, Northeast Electric Power University, Jilin City 132012, P. R. China*

Complete contact information is available at: https://pubs.acs.org/10.1021/acsomega.3c05548

Author Contributions

♦J.Z., M.H., and D.Z. contributed equally to this work.

https://doi.org/10.1021/acsomega.3c05548
ACS Omega 2023, 8, 46589−46597

Notes

The authors declare no competing financial interest.

■ ACKNOWLEDGMENTS

We acknowledge Dr. Zhiyuan Zhang and Dr. Jiarui Li for their valuable discussion and Lili Wen for making English language corrections in this paper. We acknowledge the support of the NHC Key Laboratory of Nuclear Technology Medical Transformation (Mianyang Central Hospital) (grant nos. 2021HYX010 and 2022HYX002), the National Science Foundation of China (under grant no. 11904049), and the Project funded by the China Postdoctoral Science Foundation (2019M653365 and 2022T150715).

■ REFERENCES

(1) Nonhebel, D. C.; Walton, J. C. *Free-Radical Chemistry: Structure and Mechanism*; Cambridge University Press: London, 1974.
(2) Cheeseman, K. H.; Slater, T. F. An Introduction to Free Radical Biochemistry. *Br. Med. Bull.* **1993**, *49*, 481−493.
(3) Rüchardt, C. Relations between Structure and Reactivity in Free-Radical Chemistry. *Angew Chem. Int. Ed. Engl.* **1970**, *9*, 830−843.
(4) Gutowski, M.; Kowalczyk, S. A Study of Free Radical Chemistry: Their Role and Pathophysiological Significance. *Acta Biochim. Pol.* **2013**, *60*, 1−16.
(5) Matyjaszewski, K. Preparation and Degradation of Polysilylenes. *J. Inorg. Organomet. Polym.* **1991**, *1*, 463−485.
(6) Garrison, J. B.; Hughes, R. W.; Sumerlin, B. S. Backbone Degradation of Polymethacrylates Via Metal-Free Ambient-Temperature Photoinduced Single-Electron Transfer. *ACS Macro Lett.* **2022**, *11*, 441−446.
(7) Bracco, P.; Costa, L.; Luda, M. P.; Billingham, N. A Review of Experimental Studies of the Role of Free-Radicals in Polyethylene Oxidation. *Polym. Degrad. Stab.* **2018**, *155*, 67−83.
(8) Yousufzai, A. H. K.; Zafar, M. M.; Shabih ul, H. Radical Degradation of Polyvinyl Chloride. *Eur. Polym. J.* **1972**, *8*, 1231−1236.
(9) Gröllmann, U.; Schnabel, W. Free Radical-Induced Oxidative Degradation of Polyacrylamide in Aqueous Solution. *Polym. Degrad. Stab.* **1982**, *4*, 203−212.
(10) Zhu, Y.; Zhang, D.; Zhang, Z.; Wang, Z. The Effect of Polymer Structures on Complete Degradation: A First-Principles Study. *ChemistryOpen* **2018**, *7*, 463−466.
(11) Chen, L.; Zhao, S.; Yang, Y.; Li, L.; Wang, D. Study on Degradation of Oily Wastewater by Immobilized Microorganisms with Biodegradable Polyacrylamide and Sodium Alginate Mixture. *ACS Omega* **2019**, *4*, 15149−15157.
(12) Kurenkov, V. F.; Hartan, H.-G.; Lobanov, F. I. Application of Polyacrylamide Flocculants for Water Treatment. *Chem. Comput. Simul. Butl. Commun.* **2002**, *3*, 31−40.
(13) Pearse, M. J. An Overview of the Use of Chemical Reagents in Mineral Processing. *Miner. Eng.* **2005**, *18*, 139−149.
(14) Lu, S.; Liu, R.; Sun, X. A Study on the Synthesis and Application of an Inverse Emulsion of Amphoteric Polyacrylamide as a Retention Aid in Papermaking. *J. Appl. Polym. Sci.* **2002**, *84*, 343−350.
(15) Yang, T.-H. Recent Applications of Polyacrylamide as Biomaterials. *Recent Pat. Mater. Sci.* **2008**, *1*, 29−40.
(16) Yang, M.-H. On the Thermal Degradation of Poly(Styrene Sulfone)S. V. Thermogravimetric Kinetic Simulation of Polyacrylamide Pyrolysis. *J. Appl. Polym. Sci.* **2002**, *86*, 1540−1548.
(17) Vijayalakshmi, S. P.; Madras, G. Photocatalytic Degradation of Poly(Ethylene Oxide) and Polyacrylamide. *J. Appl. Polym. Sci.* **2006**, *100*, 3997−4003.
(18) Smith, E. A.; Prues, S. L.; Oehme, F. W. Environmental Degradation of Polyacrylamides. *Ecotoxicol. Environ. Saf.* **1997**, *37*, 76−91.
(19) Al-Sabahi, J.; Bora, T.; Claereboudt, M.; Al-Abri, M.; Dutta, J. Visible Light Photocatalytic Degradation of Hpam Polymer in Oil Produced Water Using Supported Zinc Oxide Nanorods. *Chem. Eng. J.* **2018**, *351*, 56−64.
(20) Yongrui, P.; Zheng, Z.; Bao, M.; Li, Y.; Zhou, Y.; Sang, G. Treatment of Partially Hydrolyzed Polyacrylamide Wastewater by Combined Fenton Oxidation and Anaerobic Biological Processes. *Chem. Eng. J.* **2015**, *273*, 1−6.
(21) Staggs, J. E. J. Modelling Random Scission of Linear Polymers. *Polym. Degrad. Stab.* **2002**, *76*, 37−44.
(22) Emsley, A. M.; Heywood, R. J. Computer Modelling of the Degradation of Linear Polymers. *Polym. Degrad. Stab.* **1995**, *49*, 145−149.
(23) Bose, S. M.; Git, Y. Mathematical Modelling and Computer Simulation of Linear Polymer Degradation: Simple Scissions. *Macromol. Theory Simul.* **2004**, *13*, 453−473.
(24) Liu, H.; Bu, Y.; Sanjayan, J. G.; Nazari, A.; Shen, Z. Suitability of Polyacrylamide Superabsorbent Polymers as the Internal Curing Agent of Well Cement. *Constr. Build. Mater.* **2016**, *112*, 253−260.
(25) Nie, R.-c.; Guo, L.-y.; Xu, C.-y. Study on Synthesis and Flocculation Property of Cation-Polyacrylamide. *J. Coal Sci. Eng.* **2008**, *14*, 143−146.
(26) Ma, J.; Fu, K.; Fu, X.; Guan, Q.; Ding, L.; Shi, J.; Zhu, G.; Zhang, X.; Zhang, S.; Jiang, L. Flocculation Properties and Kinetic Investigation of Polyacrylamide with Different Cationic Monomer Content for High Turbid Water Purification. *Sep. Purif. Technol.* **2017**, *182*, 134−143.
(27) Perdew, J. P.; Burke, K.; Ernzerhof, M. Generalized Gradient Approximation Made Simple. *Phys. Rev. Lett.* **1996**, *77*, 3865−3868.
(28) Becke, A. D. A New Mixing of Hartree−Fock and Local Density-Functional Theories. *J. Chem. Phys.* **1993**, *98*, 1372−1377.
(29) Zhao, Y.; Truhlar, D. G. The M06 Suite of Density Functionals for Main Group Thermochemistry, Thermochemical Kinetics, Noncovalent Interactions, Excited States, and Transition Elements: Two New Functionals and Systematic Testing of Four M06-Class Functionals and 12 Other Functionals. *Theor. Chem. Acc.* **2008**, *120*, 215−241.
(30) Tao, J.; Perdew, J. P.; Staroverov, V. N.; Scuseria, G. E. Climbing the Density Functional Ladder: Nonempirical Meta−Generalized Gradient Approximation Designed for Molecules and Solids. *Phys. Rev. Lett.* **2003**, *91*, 146401.
(31) Tawada, Y.; Tsuneda, T.; Yanagisawa, S.; Yanai, T.; Hirao, K. A Long-Range-Corrected Time-Dependent Density Functional Theory. *J. Chem. Phys.* **2004**, *120*, 8425−8433.
(32) Zhen, J.-p.; Wei, X.-c.; Shi, W.-j.; Huang, Z.-y.; Jin, B.; Zhou, Y.-k. Cooperativity effect involving drug−DNA/RNA intermolecular interaction: A B3LYP-D3 and MP2 theoretical investigation on ketoprofen···cytosine···H_2O system. *J. Biomol. Struct. Dyn.* **2018**, *36*, 3587−3606.
(33) Li, J.; Zhao, F.; Jing, F.; Xiao, H. A Theoretical Study of Intermolecular Interaction of HNO3 Dimer. *J. Mol. Struct.* **2001**, *574*, 213−220.
(34) Liu, Y. J.; Huang, M. B. Hyperfine Structure of Some Hydrocarbon Radical Cations: A B3LYP and MP2 Study. *J. Mol. Struct.* **2001**, *536*, 133−142.
(35) Liang, Z.; Li, T.; Kim, M.; Asthagiri, A.; Weaver, J. F. Low-Temperature Activation of Methane on the IrO2(110) Surface. *Science* **2017**, *356*, 299−303.
(36) Zhu, D.-X.; Xia, H.; Liu, J.-G.; Chung, L. W.; Xu, M.-H. Regiospecific and Enantioselective Arylvinylcarbene Insertion of a C−H Bond of Aniline Derivatives Enabled by a Rh(I)-Diene Catalyst. *J. Am. Chem. Soc.* **2021**, *143*, 2608−2619.
(37) Wang, H.; Zhang, R.; Zhang, Q.; Zi, W. Synergistic Pd/Amine-Catalyzed Stereodivergent Hydroalkylation of 1,3-Dienes with Aldehydes: Reaction Development, Mechanism, and Stereochemical Origins. *J. Am. Chem. Soc.* **2021**, *143*, 10948−10962.
(38) Becke, A. D. Density-Functional Thermochemistry. Iii. The Role of Exact Exchange. *J. Chem. Phys.* **1993**, *98*, 5648−5652.

https://doi.org/10.1021/acsomega.3c05548
ACS Omega 2023, 8, 46589−46597

(39) Grimme, S.; Antony, J.; Ehrlich, S.; Krieg, H. A Consistent and Accurate Ab Initio Parametrization of Density Functional Dispersion Correction (Dft-D) for the 94 Elements H-Pu. *J. Chem. Phys.* **2010**, *132*, 154104.
(40) Zhu, Y.; Wang, R.; Xie, W.; Zhang, D.; Zhang, Z.; Wang, Z. An Effective Method to Make Polymers Degrade Readily: Spatial Isomerization. *Phys. Chem. Chem. Phys.* **2019**, *21*, 16905−16909.
(41) McLean, A. D.; Chandler, G. S. Contracted Gaussian Basis Sets for Molecular Calculations. I. Second Row Atoms, Z = 11−18. *J. Chem. Phys.* **1980**, *72*, 5639−5648.
(42) Krishnan, R.; Binkley, J. S.; Seeger, R.; Pople, J. A. Self-Consistent Molecular Orbital Methods. Xx. A Basis Set for Correlated Wave Functions. *J. Chem. Phys.* **1980**, *72*, 650−654.
(43) Marenich, A. V.; Cramer, C. J.; Truhlar, D. G. Universal Solvation Model Based on Solute Electron Density and on a Continuum Model of the Solvent Defined by the Bulk Dielectric Constant and Atomic Surface Tensions. *J. Phys. Chem. B* **2009**, *113*, 6378−6396.
(44) Fukui, K. Formulation of the Reaction Coordinate. *J. Phys. Chem.* **1970**, *74*, 4161−4163.
(45) Gonzalez, C.; Schlegel, H. B. Reaction Path Following in Mass-Weighted Internal Coordinates. *J. Phys. Chem.* **1990**, *94*, 5523−5527.
(46) Frisch, M. J.; Trucks, G. W.; Schlegel, H. B.; Scuseria, G. E.; Robb, M. A.; Cheeseman, J. R.; Scalmani, G.; Barone, V.; Mennucci, B.; Petersson, G. A.; Nakatsuji, H.; Caricato, M.; Li, X.; Hratchian, H. P.; Izmaylov, A. F.; Bloino, J.; Zheng, G.; Sonnenberg, J. L.; Hada, M.; Ehara, M.; Toyota, K.; Fukuda, R.; Hasegawa, J.; Ishida, M.; Nakajima, T.; Honda, Y.; Kitao, O.; Nakai, H.; Vreven, T.; Montgomery, Jr., J. A.; Peralta, J. E.; Ogliaro, F.; Bearpark, M.; Heyd, J. J.; Brothers, E.; Kudin, K. N.; Staroverov, V. N.; Kobayashi, R.; Normand, J.; Raghavachari, K.; Rendell, A.; Burant, J. C.; Iyengar, S. S.; Tomasi, J.; Cossi, M.; Rega, N.; Millam, J. M.; Klene, M.; Knox, J. E.; Cross, J. B.; Bakken, V.; Adamo, C.; Jaramillo, J.; Gomperts, R.; Stratmann, R. E.; Yazyev, O.; Austin, A. J.; Cammi, R.; Pomelli, C.; Ochterski, J. W.; Martin, R. L.; Morokuma, K.; Zakrzewski, V. G.; Voth, G. A.; Salvador, P.; Dannenberg, J. J.; Dapprich, S.; Daniels, A. D.; Farkas, O.; Foresman, J. B.; Ortiz, J. V.; Cioslowski, J.; Fox, D. J. *Gaussian 09*. revision D.01; Gaussian, Inc.: Wallingford, CT, 2009.

https://doi.org/10.1021/acsomega.3c05548
ACS Omega 2023, 8, 46589−46597